BMC Medical Imaging

RESEARCH Open Access

Development and validation of a deep learning algorithm for prediction of pediatric recurrent intussusception in ultrasound images and radiographs

Yu-feng Qian[1] and Wan-liang Guo[1*]

Abstract

Purposes To develop a predictive model for recurrent intussusception based on abdominal ultrasound (US) images and abdominal radiographs.

Methods A total of 3665 cases of intussusception were retrospectively collected from January 2017 to December 2022. The cohort was randomly assigned to training and validation sets at a 6:4 ratio. Two types of images were processed: abdominal grayscale US images and abdominal radiographs. These images served as inputs for the deep learning algorithm and were individually processed by five detection models for training, with each model predicting its respective categories and probabilities. The optimal models were selected individually for decision fusion to obtain the final predicted categories and their probabilities.

Results With US, the VGG11 model showed the best performance, achieving an area under the receiver operating characteristic curve (AUC) of 0.669 (95% CI: 0.635–0.702). In contrast, with radiographs, the ResNet18 model excelled with an AUC of 0.809 (95% CI: 0.776–0.841). We then employed two fusion methods. In the averaging fusion method, the two models were combined to reach a diagnostic decision. Specifically, a soft voting scheme was used to average the probabilities predicted by each model, resulting in an AUC of 0.877 (95% CI: 0.846–0.908). In the stacking fusion method, a meta-model was built based on the predictions of the two optimal models. This approach notably enhanced the overall predictive performance, with LightGBM emerging as the top performer, achieving an AUC of 0.897 (95% CI: 0.869–0.925). Both fusion methods demonstrated excellent performance.

Conclusions Deep learning algorithms developed using multimodal medical imaging may help predict recurrent intussusception.

Clinical trial number Not applicable.

Keywords Intussusception, Recurrence, Prediction model, Deep learning

*Correspondence:
Wan-liang Guo
gwlsuzhou@163.com
[1]Department of Radiology, Children's Hospital of Soochow University, Suzhou, China

Background

Recurrent intussusception refers to patients experiencing symptoms again after successful reduction through air enema or surgical treatment, as confirmed by abdominal ultrasound (US) or other techniques [1], and it often manifests as acute bowel obstruction. Among the numerous pediatric emergency abdominal patients, the incidence rate of intussusception in Chinese children is 418 per 100,000, surpassing the global average of 74 per 100,000. Recurrent intussusception is not uncommon with an incidence rate ranging from 8–20% [2–4], meaning that 1–2 out of every 10 children who initially experience the condition may develop it again. Although prior studies have reported that pathological lead points, such as Meckel's diverticulum, duplication, polyps, and tumors, can lead to recurrent intussusception in children [5–7], the exact mechanisms of recurrence are not fully understood.

Despite prior studies exploring risk factors for recurrent intussusception based on demographic and clinical characteristics [8], less than one-third of patients exhibit the classical triad of symptoms (abdominal pain, palpable mass, and bloody stool) [9], and certain pediatric ailments exhibit similar clinical presentations. Further, early physical examination may yield negative results [1]. Hence, diagnosis can often be delayed or overlooked during the initial emergency visit. Any delay in the proper diagnosis and treatment of such cases can lead to severe complications, such as bowel ischemia, necrosis, and perforation, which may necessitate intestinal resection [2, 10, 11]. This poses significant challenges for most pediatricians, radiologists, and pediatric surgeons in predicting and preventing intussusception recurrence in clinical practice.

In recent years, there has been increased interest in the application of deep learning algorithms for image recognition and disease prediction [12–14]. Convolutional neural networks, including LeNet-5, AlexNet, VGGNet, and GoogleNet, have been proposed and applied in medical imaging (such as computer-aided diagnosis) [15–17]. Deep learning techniques leverage the exponential growth of computing power to learn autonomously and extract abstract and complex features from pixel-level imaging data [18].

The aim of this study is to establish a predictive model for recurrent intussusception based on radiographic images of initial intussusception in a cohort of patients. Such a model seeks to enhance the efficiency of clinical physicians by alerting them to potential intussusception recurrence, thereby preventing adverse events.

Material and method

Patients

This retrospective study received approval from the Institutional Review Board (IRB) of the Children's Hospital of Soochow University, with the requirement for informed consent waived. The authors had complete access to and control over all of the data in the study, and no conflicts of interest were reported.

The final diagnosis of intussusception was made using ultrasound combined with air enema or surgery. For those confirmed with intussusception, air enema reduction was the primary treatment method. If the intussusception was not successfully reduced after three attempts, surgical intervention was required. Recurrent intussusception was defined as the recurrence of intussusception after air enema reduction or surgery. Non-recurrent intussusception was defined as the cases that were successfully reduced after air enema or surgery without recurrence [19, 20]. The dataset of this study was retrieved from the institutional picture archiving and communication systems (PACS) database for medical records from January 2017 and December 2022. A total of 4818 consecutive children were diagnosed with intussusception, of which 4631 intussusception cases occurred in the right abdomen, resulting in a probability of approximately 96.1%. Given this high frequency, we focused on the recurrence of intussusception at this location.

The inclusion criteria were as follows: (1) availability of clinical data; (2) intussusception cases that occurred in the right abdomen. The exclusion criteria were as follows: (1) patients lacking abdominal US or abdominal x-ray imaging, (2) those with a history of intestinal surgery before, and (3) cases with inadequate image quality such as motion artifacts and overlapping shadows. Note that recurrent patients may have multiple ultrasounds and X-rays, we admitted the images from the first occurrence of intussusception.

Finally, we retrospectively enrolled 3665 children with intussusception in the study, comprising 2968 non-recurrent patients and 697 recurrent patients. These patients were then randomly divided into two groups at a 6:4 ratio: the training cohort ($n = 2199$) and the validation cohort ($n = 1466$). The inclusion criteria and exclusion criteria, as well as patient grouping, are shown in Fig. 1.

US images and radiographs acquisition

US examinations were performed using five different US systems, including GE, Philips, Toshiba Aplio 400, VINNO 70, and SIEMENS. All ultrasound scans were performed by three radiologists with more than 3 years of diagnostic experience. The child was placed in a supine position. Both the linear array probe and the convex array probe were used to scan the entire abdominal cavity thoroughly. When anomalies were detected, longitudinal

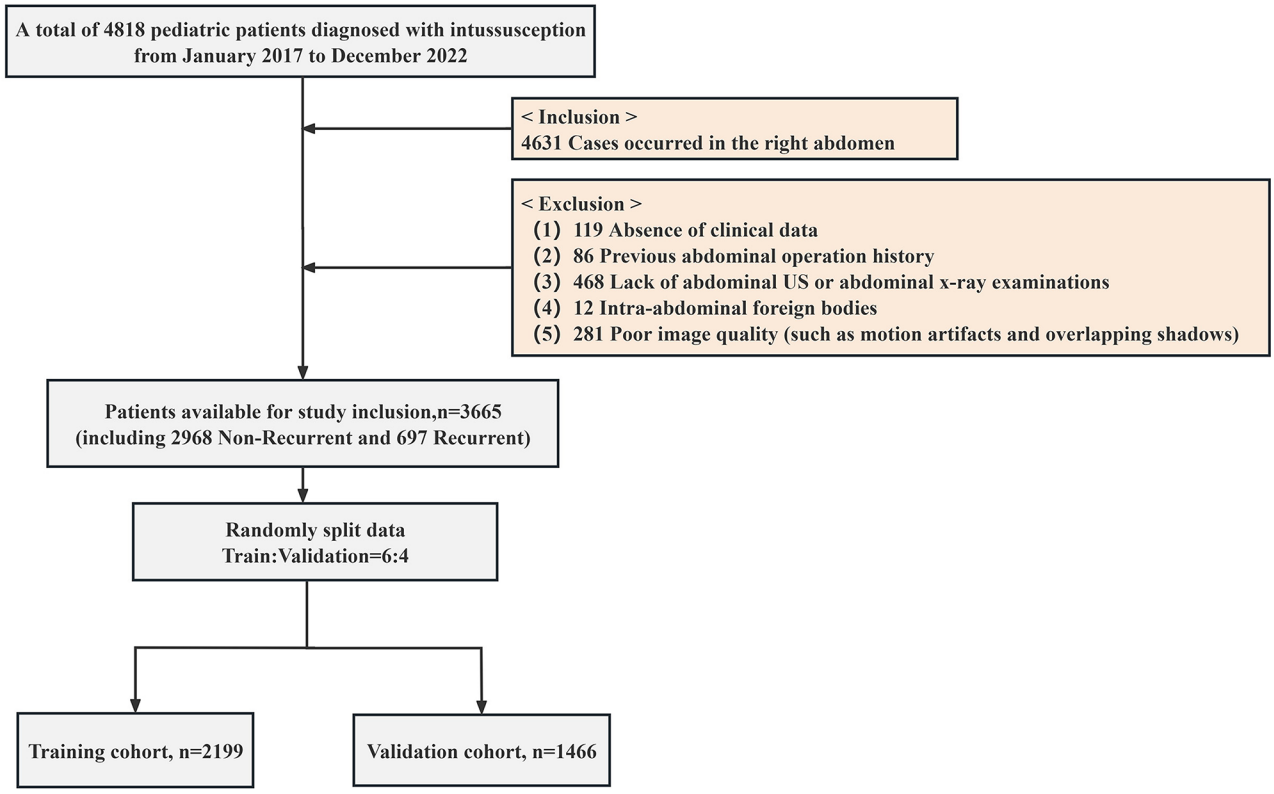

Fig. 1 Flowchart shows inclusion criteria and exclusion criteria

and transverse multi-sectional scans were performed to observe the lesions in real time as the child's position changed. Once the lesions were distinctly visualized, the location of the mass was recorded, the diameter of the "concentric circle" sign and the length of the "sleeve sign" were measured [21]. The static grayscale image was stored in DICOM format within the PACS.

All of the x-ray examinations were performed using a Shimadzu RF system. Pediatric patients underwent abdominal anteroposterior x-ray imaging in a calm breathing state before air enema. These images were also stored in DICOM format using the PACS.

After image quality control conducted by two radiologists (Q.Y. and G.W.), images that met the inclusion criteria were converted to PNG format. We smoothed the images by averaging the pixel values of neighboring pixels within a defined area around each pixel. This effectively reduced random noise in the images.

Region of interest segmentation

For the US images, the regions of interest (ROIs) were manually delineated by placing bounding boxes around the invagination region associated with intussusception. Specifically, the ROI for each lesion was defined as the smallest rectangular area that encompassed the entire lesion. For the X-ray images, the ROIs were defined as rectangular areas extending from the level of the right diaphragm to the level of the right iliac crest, laterally to the outer edges of the vertebral bodies. The aim of this approach is to minimize the influence of unnecessary factors, such as the vertebral bodies and iliac bones, thereby enabling the subsequent deep learning algorithm to concentrate more effectively on the condition of the right intestinal tract. The ROIs were drawn by a radiologist with 5 years of experience using open-source annotation tools LabelImg. To assess the segmentation availability, another radiologist with 10 years of experience reviewed the image segmentation. If any ROI was questioned, re-segmentation would be performed following mutual agreement between the two radiologists.

Deep learning models development

The transfer learning models used in this study included ResNet 18, VGG 11, MobileNet V2, Inception V3 and AlexNet. All of them are pretrained on the ImageNet dataset and have demonstrated effective performance in classification tasks. Before training, the subregion images of the region of interest were cropped and were resized to 299×299 pixels for Inception V3 and 224×224 pixels for the other CNN models, and z-score normalization was applied to all images. The obtained images were used as inputs for deep learning network structures to develop the predictive models for intussusception recurrence. We fixed the fully connected layers. And the last output layer

of the structure was modified to add a sigmoid activation function to make it available for two classifications. The stochastic gradient descent (SGD) optimizer was used to update the model parameters with an initial learning rate of 0.01, for a total of 50 epochs, and a batch size of 32. We employed a batch balance technique to address the imbalance between recurrent and non-recurrent intussusception cases during the upsampling process. Specifically, we ensured that each batch contained an equal number of recurrent and non-recurrent cases, maintaining a 1:1 ratio. Model training was conducted on a system equipped with an NVIDIA GeForce RTX 4070ti GPU.

Construction of the fusion model

The current study utilized two fusion strategies to develop the fusion model. In the first strategy, the two models were combined into an ensemble by using a soft voting scheme of averaging the probabilities from the models to fuse the decision of individual models. In the second strategy, we employed the stacking ensemble learning strategy to integrate the output probabilities from the two basic models. We employed six stacking models including SVM, KNN, RandomForest, ExtraTrees, LightGBM, XGBoost to determine the most effective model for our task. The flow diagram of this study is illustrated in Fig. 2.

Statistical analysis

All of the statistical analyses were performed using IBM SPSS Statistics 27; calculations were performed with 95% confidence intervals (CIs). A p value < 0.05 was considered to be statistically significant. The Kolmogorov–Smirnov test was employed to confirm the normal distribution of all of the datasets. The independent t-test or the Kruskal–Wallis test was employed to identify differences in clinical features between the recurrent intussusception group and the non-recurrent intussusception group. All of the data were presented as numbers (n) and percentages. Continuous variables were represented as mean ± standard deviation, while discrete variables were represented as counts (percentages). The performances of different models were evaluated using accuracy, sensitivity, specificity, and the area under the receiver operating characteristic curve (AUC). Decision curve analysis (DCA) quantified the net benefits at various threshold probabilities, allowing for an assessment of the models' clinical efficiency in predicting recurrent intussusception.

Results

Characteristics of patients

In the retrospective datasets, a total of 3665 (M: F = 2368:1297; mean age: 24.92 ± 16.63 months) children with intussusception were included in the analysis, with 2199 (M: F = 1442:757; mean age: 25.03 ± 16.64months) classified in the training set and 1466 (M: F = 926:540;

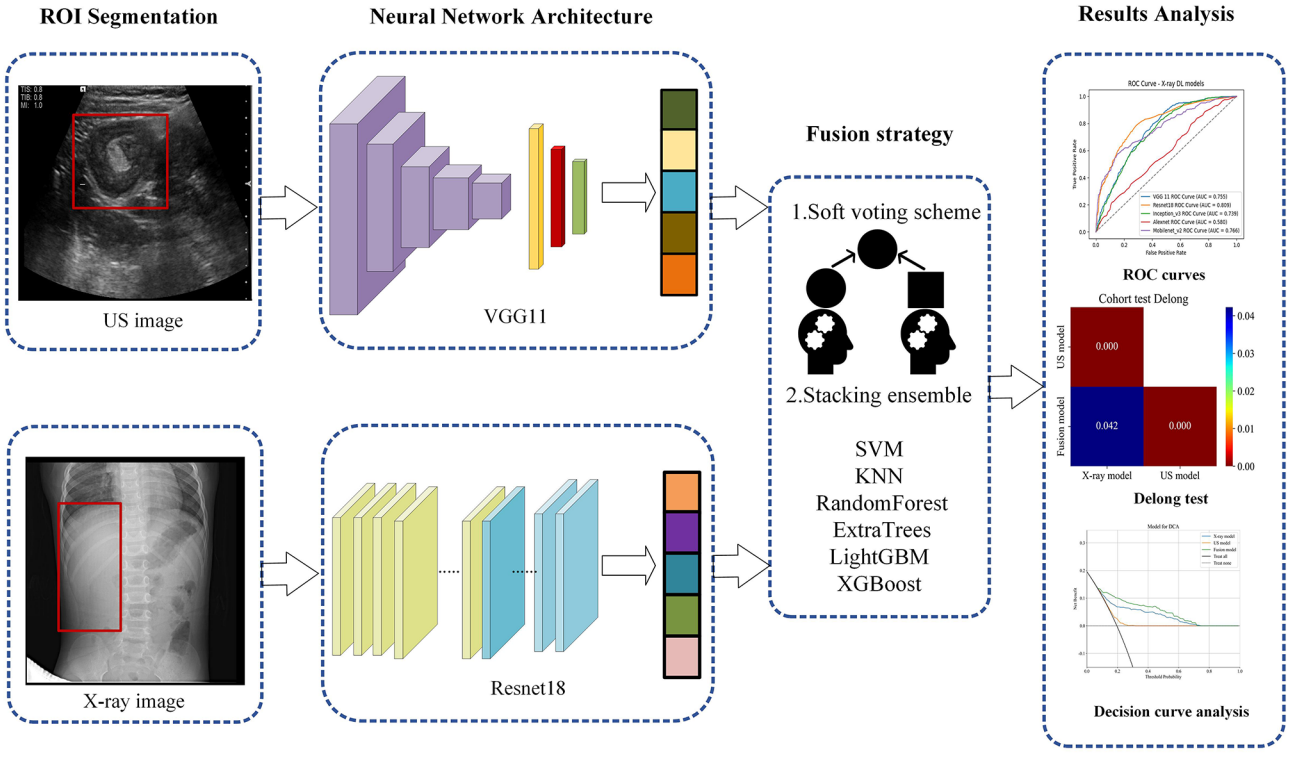

Fig. 2 Acquisition and pre-processing of US images and radiographs, as well as the flow diagram of this study

Table 1 Demographic and clinical characteristics of patients

Characteristics	A retrospective dataset			
	All	Training set	Validation set	*P* value
Number of patients	3665	2199	1466	
Final diagnosis N (%)				
Non-recurrent intussusception	2968(80.98)	1789(81.36)	1189(81.11)	
Recurrent intussusception	697(19.02)	410(18.64)	287(18.89)	
Patients' characteristics				
Age (Month)	24.92 ± 16.63	25.03 ± 16.64	24.75 ± 16.61	0.5748
Gender N (male %)	2368(64.61)	1442(65.58)	926(63.17)	0.1443
Patients' clinical symptoms N (%)				
Abdominal pain	2686(73.29)	1610(73.22)	1076(73.40)	0.9331
Cry and scream	1800(49.11)	1066(48.48)	734(50.07)	0.3625
Vomit	2349(64.09)	1413(64.26)	936(63.85)	0.8275
Bloody stools	905(24.69)	547(24.87)	358(24.42)	0.7843
Abdominal mass	781(21.31)	450(20.46)	331(22.58)	0.1361
Fever	370(10.10)	213(9.69)	157(10.71)	0.3414
Diarrhea	137(3.74)	74(3.37)	63(4.30)	0.1711
Enlarged lymph nodes	426(11.62)	258(11.73)	168(11.46)	0.8415
Abdominal and pelvic effusion	103(2.81)	70(3.18)	33(2.25)	0.1162
Pathologic lead points	27(0.74)	17(0.77)	10(0.68)	0.9058
Mass size (mm)				
Length	35.15 ± 4.95	35.19 ± 5.02	35.08 ± 4.84	0.4608
Width	30.85 ± 4.14	30.87 ± 4.22	30.83 ± 4.01	0.6525

N = Number of patients or images, mm = millimeter. Data are presented as n (%) or mean ± standard deviation

mean age: 24.75 ± 16.61 months) in the validation set. All of the children underwent abdominal US scans and abdominal x-ray examinations. The demographic and clinical characteristics of patients in the training and validation datasets are presented in Table 1. There were no significant differences in samples between groups ($P > 0.05$).

Performance analysis of the US, X-ray deep learning models and the fusion models

The ROC curers and AUCs of the five deep learning models in the validation set were presented in Fig. 3. For the US model, the overall performance of VGG11 was relatively better than that of the other CNNs in both training set and validation set (Table 2). The VGG11 achieved the highest performance with an AUC of 0.669 (95% CI: 0.635–0.702), accuracy of 0.589, sensitivity of 0.672, specificity of 0.569 in the validation set, as shown in Fig. 4a. However, for the X-ray model, the ResNet18 model exhibited superior overall performance in two sets (Table 3), achieving an AUC of 0.809 (95% CI: 0.776–0.841), accuracy of 0.73, sensitivity of 0.779, specificity of 0.718 in the validation set, as shown in Fig. 4b. The PPV of the individual US and X-ray model was suboptimal, particularly the US model, which had a PPV of only 0.275. This may be attributed to the issue of data imbalance, as it often causes the model to be biased towards the majority class. In contrast, the fusion models demonstrate superior performance, with an increase in PPV. The soft voting scheme revealed an AUC of 0.877 (95% CI: 0.846–0.908), accuracy of 0.820, sensitivity of 0.721, specificity of 0.843, PPV of 0.519 and NPV of 0.928. For the stacking ensemble strategy, all six machine learning models exhibited strong performance in the validation set, with LightGBM delivering the best overall results. It

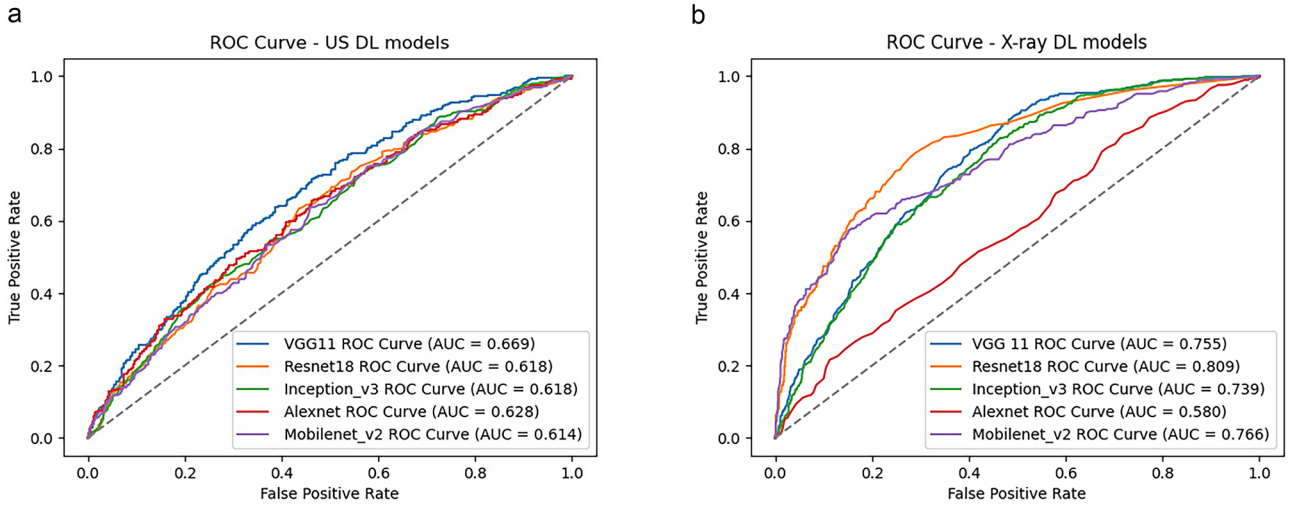

Fig. 3 The ROC curves of different deep learning models for predicting recurrent intussusception in the validation cohort. (**a**) The ROC curves of different US models. (**b**) The ROC curves of different X-ray models

Table 2 Performances of the US predictive models in the training and validation sets

Model Name	Accuracy	AUC	95% CI	Sensitivity	Specificity	PPV	NPV	F1	Threshold	Cohort
VGG11	0.796	0.866	0.8479–0.8847	0.751	0.806	0.482	0.931	0.578	0.217	Train
VGG11	0.589	0.669	0.6353–0.7025	0.672	0.569	0.275	0.878	0.391	0.125	Validation
ResNet18	0.797	0.843	0.8218–0.8650	0.705	0.818	0.482	0.920	0.591	0.400	Train
ResNet18	0.579	0.618	0.5828–0.6534	0.624	0.568	0.258	0.863	0.367	0.112	Validation
Inception_v3	0.702	0.811	0.7883–0.8334	0.778	0.684	0.372	0.928	0.493	0.181	Train
Inception_v3	0.671	0.618	0.5830–0.6539	0.439	0.727	0.279	0.844	0.343	0.219	Validation
Alexnet	0.686	0.838	0.8172–0.8582	0.846	0.650	0.368	0.946	0.501	0.149	Train
Alexnet	0.566	0.628	0.5921–0.6640	0.624	0.552	0.251	0.859	0.360	0.269	Validation
Mobilenet_v2	0.761	0.832	0.8116–0.8530	0.710	0.772	0.428	0.917	0.525	0.209	Train
Mobilenet_v2	0.559	0.614	0.5784–0.6490	0.620	0.544	0.246	0.856	0.355	0.080	Validation

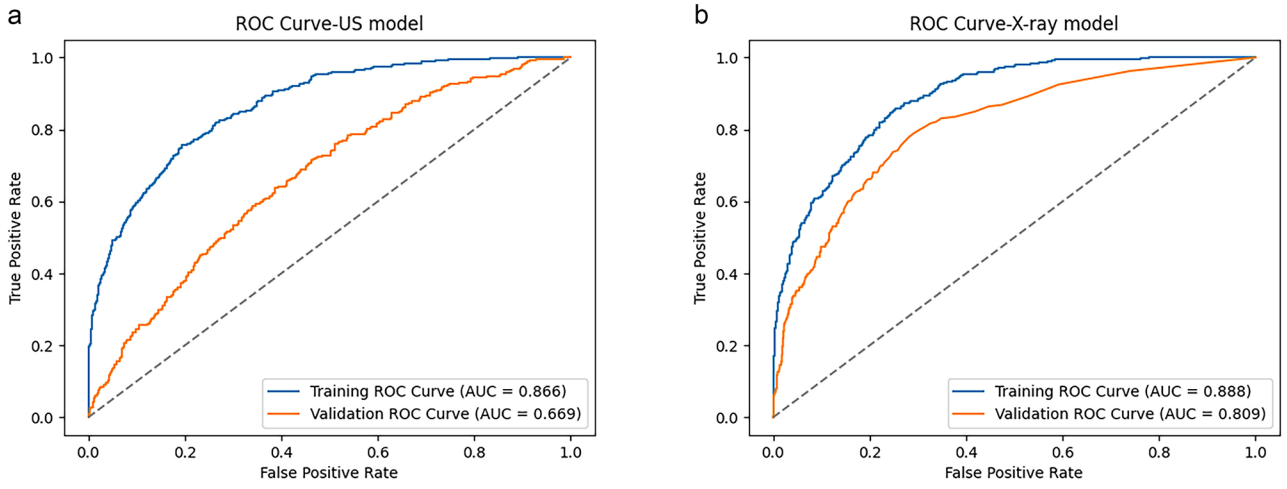

Fig. 4 ROC curves show the performance of the two optimal models. (**a**) Performance of VGG11 model with US. (**b**) Performance of ResNet18 model with radiographs

Table 3 Performances of the X-ray predictive models in the training and validation sets

Model Name	Accuracy	AUC	95% CI	Sensitivity	Specificity	PPV	NPV	F1	Threshold	Cohort
VGG11	0.801	0.864	0.8402–0.8883	0.784	0.805	0.580	0.949	0.606	0.117	Train
VGG11	0.611	0.755	0.7344–0.7823	0.839	0.559	0.369	0.369	0.446	0.179	Validation
ResNet18	0.769	0.888	0.8733–0.9024	0.851	0.750	0.617	0.942	0.769	0.888	Train
ResNet18	0.730	0.809	0.7762–0.8414	0.779	0.718	0.473	0.927	0.730	0.809	Validation
Inception_v3	0.834	0.868	0.8413–0.8940	0.784	0.846	0.597	0.597	0.649	0.097	Train
Inception_v3	0.602	0.739	0.7345–0.7819	0.824	0.551	0.351	0.888	0.436	0.175	Validation
Alexnet	0.615	0.751	0.7275–0.7751	0.820	0.568	0.367	0.893	0.442	0.177	Train
Alexnet	0.394	0.580	0.5432–0.6159	0.829	0.288	0.180	0.803	0.349	0.168	Validation
Mobilenet_v2	0.842	0.870	0.8436–0.8962	0.763	0.861	0.603	0.959	0.654	0.110	Train
Mobilenet_v2	0.598	0.766	0.7193–0.7670	0.837	0.543	0.375	0.890	0.431	0.174	Validation

achieved an AUC of 0.897 (95% CI: 0.869–0.925), accuracy of 0.806, sensitivity of 0.800, specificity of 0.808, PPV of 0.501 and NPV of 0.945. More details were shown in Table 4. The ROC curves of three prediction models were shown in Fig. 5. To evaluate the effectiveness of the models, the Delong test (Fig. 6) was performed. The results showed that the AUC of the fusion model was significantly superior to both the US model ($P<0.001$) and the X-ray model ($P=0.042$) in the testing cohort. This indicates that the fusion model demonstrated the highest level of diagnostic efficacy. The DCAs of the three models are presented in Fig. 7. The results demonstrate that the fusion model provided the greatest net benefit in predicting recurrent intussusception in the validation set.

Discussion

Nowadays, the early diagnosis and management of recurrent intussusception pose challenges for pediatricians. In this study, we developed prediction models for recurrent intussusception based on US and X-ray images,

Table 4 The performance of stacking ensemble strategy and soft voting strategy in the validation set

Model Name	Accuracy	AUC	95% CI	Sensitivity	Specificity	PPV	NPV	F1	Threshold
Stacking									
SVM	0.876	0.829	0.7824–0.8749	0.671	0.924	0.674	0.923	0.674	0.122
KNN	0.862	0.838	0.7992–0.8775	0.521	0.943	0.682	0.894	0.591	0.400
RandomForest	0.784	0.818	0.7748–0.8606	0.700	0.804	0.456	0.920	0.554	0.200
ExtraTrees	0.810	0.809	0.7654–0.8521	0.629	0.853	0.499	0.907	0.559	0.300
LightGBM	0.806	0.897	0.8685–0.9250	0.800	0.808	0.501	0.945	0.612	0.250
XGBoost	0.754	0.892	0.8631–0.9204	0.857	0.730	0.427	0.956	0.571	0.174
Soft voting									
Average	0.820	0.877	0.8459–0.9082	0.721	0.843	0.519	0.928	0.605	0.252

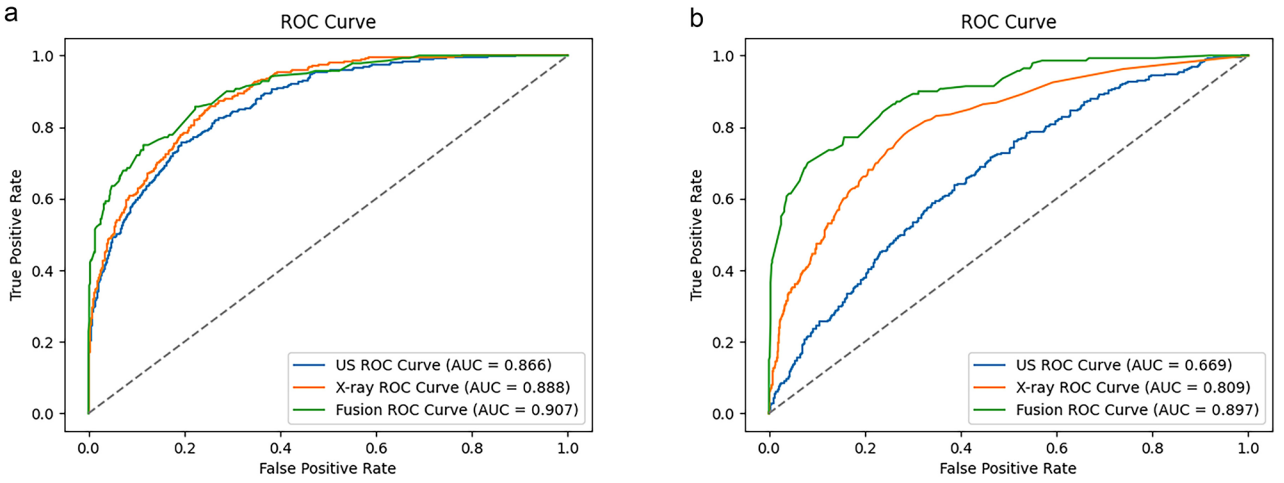

Fig. 5 ROC curves of the best three prediction models (**a**) in the training cohort and (**b**) in the validation cohort

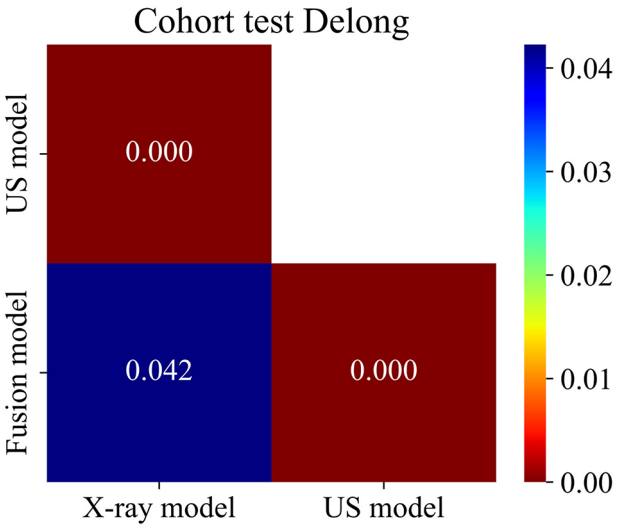

Fig. 6 Delong test between different models

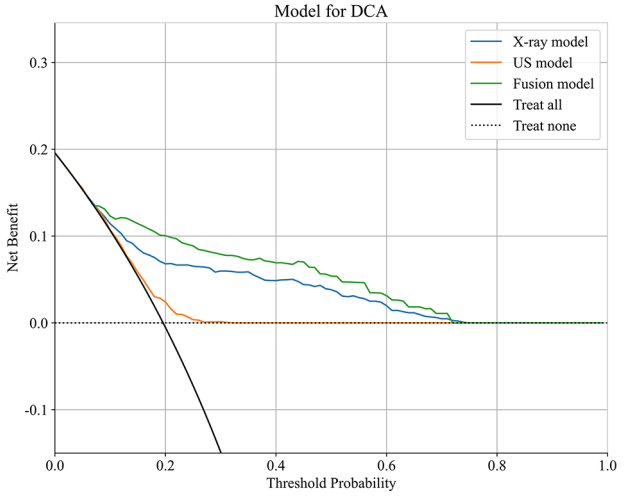

Fig. 7 The DCA curves for US model, X-ray model and fusion model in the validation cohort

respectively. We employed two fusion strategies to construct the fusion model: the soft voting scheme and stacking ensemble. The results indicated that the LightGBM stacking model achieved the highest performance, with an AUC of 0.897 in the test set.

Despite progress in deep learning for other body parts, only a few approaches focus on intussusception. Accurate and timely diagnosis of recurrent intussusception is critical for selecting treatment plans and achieving positive treatment outcomes [22–24]. Ultrasound and X-ray are important imaging modalities that are helpful not only

in the diagnosis of intussusception but also in assessing the location of the intussusception and the vascular compromise of the intestinal wall. These examinations are invaluable for evaluating intestinal conditions and informing treatment decisions. The majority of the prior studies have proposed using deep learning to diagnose intussusception in children using single types of imaging data, either abdominal radiographs [25] or abdominal US images [26]. There are some differences between our study and previous studies. Li et al., employing an improved Faster RCNN, revealed the importance of detecting "concentric circle" signs in abdominal US to diagnose pediatric intussusception [26]. Another study tested the performance of a deep learning–based algorithm to detect ileocolic intussusception using abdominal radiographs of young children, and a YOLOv3-based algorithm was developed to recognize the rectangular area of the right abdomen and to diagnose intussusception [27]. Although their results showed high diagnostic accuracy, it should be noted that the researchers used data from a single image type and have overlooked its application in recurrent intussusception. Conversely, our work focused on using larger datasets of both abdominal radiographs and abdominal US images to develop multimodal models for predicting the occurrence of recurrent intussusception. Guo et al. used machine learning models to predict recurrent cases of intussusception in children, achieving a sensitivity of 0.555, a specificity of 0.793, and an accuracy of 0.771 [19]. Compared with Guo's work, we used larger datasets and demonstrated superior performance. Our models can make predictions using imaging data alone, suggesting their applicability in clinical practice.

To the best of our knowledge, no research combines US images and radiographs to predict recurrent intussusception. Our model focuses on predicting recurrent intussusception, which is more challenging and complex than models designed for general intussusception detection. Moreover, we employed post-fusion methods to further enhance the model's performance. Advancements in deep learning for medical imaging have led to a growing interest in providing support to radiologists and clinical physicians. Its application in recurrent intussusception can help pediatric surgeons more accurately predict cases, especially those involving persistent or malignant recurrences. As the workload of medical imaging and radiologists continues to grow, advances in artificial intelligence are expected to improve diagnostic accuracy and efficiency in routine practice.

In the present study, we encountered a significant issue of data imbalance. To effectively address this challenge, we employed the batch balance technique during the sampling process. The core of this technique involves downsampling majority class samples while oversampling minority class samples, ensuring an equal number of recurrent and non-recurrent cases in each batch (1:1 ratio). This strategy effectively alleviated the issue of data imbalance to some extent. However, the PPV of the individual models remained suboptimal. In the prior studies, SMOTE has been widely utilized to address the issue of data imbalance. We chose not to employ SMOTE due to several considerations. Firstly, our US images originated from multiple machines, which may result in significant discrepancies in sample feature distributions. Consequently, the new samples generated by SMOTE might not accurately represent the true characteristics of the actual data, potentially compromising the model's generalization capability. Secondly, SMOTE is sensitive to noise and outliers, and the generated samples could introduce extraneous interference, further diminishing model performance.

There are several limitations to our study. First, it was a single-center study; multicenter evaluations are needed to further develop and validate our models. Second, it was a retrospective study with a limited dataset size; further improvements will require large-scale prospective studies. Third, due to their limited availability, CT, MRI and other types of images were not included in our study. Lastly, we did not compare the performance of our models with that of physicians' diagnoses.

In summary, we developed a multimodal deep learning fusion model for predicting recurrent intussusception, which exhibited high accuracy and reliability. This model could potentially provide surgeons with support in predicting recurrent intussusception.

Acknowledgements
None.

Author contributions
Yu-feng Qian was primarily responsible for patient screening, data collection, preliminary data analysis, and drafting the manuscript. Wan-liang Guo contributed to the study design, conducted the final data analyses and interpretation, and assisted in manuscript preparation. Both authors critically reviewed and approved the final version of the manuscript.

Funding
No funding.

Data availability
No datasets were generated or analysed during the current study.

Declarations

Ethics approval and consent to participate
This study was approved by the Medical Ethics Committee of the Children's Hospital of Soochow University. The committee waived the requirement for informed consent due to the retrospective nature of the study and the minimal risk to participants. All methods were conducted in accordance with relevant guidelines and regulations.

Consent for publication
Not applicable.

Competing interests
The authors declare no competing interests.

Received: 27 June 2024 / Accepted: 5 February 2025
Published online: 03 March 2025

References

1. Marsicovetere P, Ivatury SJ, White B, Holubar SD. Intestinal intussusception: etiology, diagnosis, and treatment[J]. Clin Colon Rectal Surg. 2017;30(1):30–9. https://doi.org/10.1055/s-0036-1593429.
2. Niramis R, Watanatittan S, Kruatrachue A, Anuntkosol M, Buranakitjaroen V, Rattanasuwan T, Wongtapradit L, Tongsin A. Management of recurrent intussusception: nonoperative or operative reduction? J Pediatr Surg. 2010;45(11):2175–80. https://doi.org/10.1016/j.jpedsurg.2010.07.029.
3. Cho MJ, Nam CW, Choi SH, Hwang EH. Management of recurrent ileocolic intussusception. J Pediatr Surg. 2020;55(10):2150–3. https://doi.org/10.1016/j.jpedsurg.2019.09.039.
4. Chen X, Chen Q, Wang X, Gao Z. Clinical characteristics of recurrent intussusception: a single-center retrospective study. J Pediatr Surg. 2021;56(10):1831–4. https://doi.org/10.1016/j.jpedsurg.2021.03.051.
5. Saka R, Sasaki T, Matsuda I, Nose S, Onishi M, Fujino T, Shimomura H, Otsuka Y, Kajimoto N, Hirota S, Oue T. Chronic ileocolic intussusception due to transmural infiltration of diffuse large B cell lymphoma in a 14-year-old boy: a case report. Springerplus. 2015;4:366. https://doi.org/10.1186/s40064-015-1157-6.
6. Dias AR, Lopes RI, do Couto RC, Bonafe WW, D'Angelo L, Salvestro ML. Ileal duplication causing recurrent intussusception. J Surg Educ. 2007;64(1):51–3. https://doi.org/10.1016/j.cursur.2006.09.003.
7. Kim KH, Kang KA, Lim JH, Lee KG, Kwon TJ. Inverted Meckel diverticulum as a lead point of small bowel intussusception: misinterpreting case as a lipoma. Clin Imaging. 2016;40(5):840–2. https://doi.org/10.1016/j.clinimag.2016.03.009.
8. Guo JY, Qian YF. Predicting recurrent cases of intussusception in children after air enema reduction with machine learning models. Pediatr Surg Int. 2022;39(1):9. https://doi.org/10.1007/s00383-022-05309-6.
9. Caruso AM, Pane A, Scanu A, Muscas A, Garau R, Caddeo F, Mascia L. Intussusception in children: not only surgical treatment. J Pediatr Neonatal Individualized Med (JPNIM). 2017;6(1):e060135. https://doi.org/10.7363/060135.
10. Edwards EA, Pigg N, Courtier J, Zapala MA, MacKenzie JD, Phelps AS. Intussusception: past, present and future. Pediatr Radiol. 2017;47(9):1101–8. https://doi.org/10.1007/s00247-017-3878-x.
11. Lehnert T, Sorge I, Till H, Rolle U. Intussusception in children–clinical presentation, diagnosis and management. Int J Colorectal Dis. 2009;24(10):1187–92. https://doi.org/10.1007/s00384-009-0730-2.
12. Litjens G, Kooi T, Bejnordi BE, Setio AAA, Ciompi F, Ghafoorian M, van der Laak JAWM, van Ginneken B, Sánchez CI. A survey on deep learning in medical image analysis. Med Image Anal. 2017;42:60–88. https://doi.org/10.1016/j.media.2017.07.005.
13. Cao C, Liu F, Tan H, Song D, Shu W, Li W, Zhou Y, Bo X, Xie Z. Deep learning and its applications in Biomedicine. Genomics Proteom Bioinf. 2018;16(1):17–32. https://doi.org/10.1016/j.gpb.2017.07.003.
14. Mazurowski MA, Buda M, Saha A, Bashir MR. Deep learning in radiology: an overview of the concepts and a survey of the state of the art with focus on MRI. J Magn Reson Imaging. 2019;49(4):939–54. https://doi.org/10.1002/jmri.26534.
15. He J, Baxter SL, Xu J, Xu J, Zhou X, Zhang K. The practical implementation of artificial intelligence technologies in medicine. Nat Med. 2019;25(1):30–6. https://doi.org/10.1038/s41591-018-0307-0.
16. Nguyen DT, Lee MB, Pham TD, Batchuluun G, Arsalan M, Park KR. Enhanced image-based endoscopic pathological site classification using an ensemble of Deep Learning models. Sens (Basel). 2020;20(21):5982. https://doi.org/10.3390/s20215982.
17. Shin HC, Roth HR, Gao M, Lu L, Xu Z, Nogues I, Yao J, Mollura D, Summers RM. Deep convolutional neural networks for computer-aided detection: CNN Architectures, dataset characteristics and transfer learning. IEEE Trans Med Imaging. 2016;35(5):1285–98. https://doi.org/10.1109/TMI.2016.2528162.
18. Alzubaidi L, Zhang J, Humaidi AJ, Al-Dujaili A, Duan Y, Al-Shamma O, Santamaría J, Fadhel MA, Al-Amidie M, Farhan L. Review of deep learning: concepts, CNN architectures, challenges, applications, future directions. J Big Data. 2021;8(1):53. https://doi.org/10.1186/s40537-021-00444-8.
19. Guo WL, Hu ZC, Tan YL, Sheng M, Wang J. Risk factors for recurrent intussusception in children: a retrospective cohort study. BMJ Open. 2017;7(11):e018604. https://doi.org/10.1136/bmjopen-2017-018604.
20. Ting X, Xufei D, Jiangbin L, Weijue X, Zhibao L, Guogang Y. Development and validation of a Nomogram for Predicting Pathological intussusceptions in Children Prior to Surgical intervention. Front Pediatr. 2022;10:877358. https://doi.org/10.3389/fped.2022.877358.
21. Henrikson S, Blane CE, Koujok K, Strouse PJ, DiPietro MA, Goodsitt MM. The effect of screening sonography on the positive rate of enemas for intussusception. Pediatr Radiol. 2003;33(3):190–3. https://doi.org/10.1007/s00247-002-0848-7.
22. Applegate KE. Intussusception in children: evidence-based diagnosis and treatment. Pediatr Radiol. 2009;39(Suppl 2):S140–3. https://doi.org/10.1007/s00247-009-1178-9.
23. Kelley-Quon LI, Arthur LG, Williams RF, Goldin AB, St Peter SD, Beres AL, Hu YY, Renaud EJ, Ricca R, Slidell MB, Taylor A, Smith CA, Miniati D, Sola JE, Valusek P, Berman L, Raval MV, Gosain A, Dellinger MB, Sømme S, Downard CD, McAteer JP, Kawaguchi A. Management of intussusception in children: a systematic review. J Pediatr Surg. 2021;56(3):587–96. https://doi.org/10.1016/j.jpedsurg.2020.09.055.
24. Waseem M, Rosenberg HK. Intussusception. Pediatr Emerg Care. 2008;24(11):793–800. https://doi.org/10.1097/PEC.0b013e31818c2a3e.
25. Kwon G, Ryu J, Oh J, Lim J, Kang BK, Ahn C, Bae J, Lee DK. Deep learning algorithms for detecting and visualising intussusception on plain abdominal radiography in children: a retrospective multicenter study. Sci Rep. 2020;10(1):17582. https://doi.org/10.1038/s41598-020-74653-1.
26. Li Z, Song C, Huang J, Li J, Huang S, Qian B, Chen X, Hu S, Shu T, Yu G. Performance of Deep Learning-based algorithm for detection of Pediatric Intussusception on Abdominal Ultrasound images. Gastroenterol Res Pract. 2022;2022:9285238. https://doi.org/10.1155/2022/9285238.
27. Kim S, Yoon H, Lee MJ, Kim MJ, Han K, Yoon JK, Kim HC, Shin J, Shin HJ. Performance of deep learning-based algorithm for detection of ileocolic intussusception on abdominal radiographs of young children. Sci Rep. 2019;9(1):19420. https://doi.org/10.1038/s41598-019-55536-6.

Publisher's note